PHYSICAL REVIEW E **87**, 020901(R) (2013)

Golden spirals as phyllotactic arrangements of optical patterns

F. Haudin[1,2] and S. Residori[1]

[1]*INLN, Université de Nice-Sophia Antipolis, CNRS, 1361 route des Lucioles 06560 Valbonne, France*

[2]*Nonlinear Physical Chemistry Unit, Faculté des Sciences, CP 231, Université Libre de Bruxelles (ULB), 1050 Brussels, Belgium*

(Received 7 October 2012; published 8 February 2013)

A nonlinear optical medium with nonlocal feedback is shown to have all the necessary ingredients to simulate a growthlike process that generates golden spirals and phyllotactic patterns. Elementary droplets of light are generated by the optical nonlinearity whereas the combination of rotation and translation in the feedback loop geometrically distributes them on spiraling patterns. The symmetry of the geometrical arrangements is described with the help of a simple replication algorithm.

DOI: 10.1103/PhysRevE.87.020901 PACS number(s): 05.45.−a, 47.54.−r, 42.65.−k

Spatial self-structuration is an ubiquitous phenomenon and nature supplies many beautiful examples of spontaneous pattern formation [1]. Particularly, the vegetal world offers some of the most striking examples, as the organizations of the sunflower seeds or the pine cone scales, described by two sets of spirals ruled by the golden number and the Fibonacci sequence. Similar growth modes have been reproduced in physics [2], numerically and experimentally, by considering elementary droplets of fluids or matter [3,4]. Geometrical and dynamical approaches have been shown to produce phyllotactic structures [2–8], whereas phyllotacticlike modes have also been obtained in convection cells [9] or in layers of superconductive materials [10]. Numerical simulations based on an elastic model have been able to reproduce a broad spectrum of phyllotactic patterns similar to those formed by the spines of cacti [2]. For a system of core/shell microstructures, particular series of Fibonacci spirals have been drawn over triangular patterns depending on the stress applied to the shells and on the geometry of the supporting surface [11,12]. Recently, a system of magnetic cacti, consisting of magnets along a cylindrical stem, has been studied both experimentally and numerically [13,14]. Concerning optical systems, the far-field properties of phase-only diffractive masks with phyllotactic arrangements have been studied experimentally [15,16]. However, there is, to the best of our knowledge, no evidence of phyllotactic patterns generated in the near field of a self-organizing optical system. Starting from this assessment, we propose here an experimental study where circular or spiraling modes of optical localized structures are induced in a nonlinear optical system with nonlocal feedback. The system is bistable and permits to locally induce localized structures that play the role of elementary "droplets" of light, while the nonlocal feedback acts as a forcing able to impose the symmetry for the phyllotactic arrangements to develop. Phyllotactic optical arrangements appear for a relatively large range of V_0 and I_{in}, here the control parameters that determine the width of the region in which optical localized structures are stable. Inside this region, localized structures can be considered as the optical analogs of the elements of a green plant. Then, the self-structuring of the equivalent "optical plant" is driven by the optical feedback, which imposes a recursive law for the disposal of adjacent elements. These phyllotactic arrangements are produced within the larger context of optical patterns, therefore, their study could aid in understanding better the special conditions required for phyllotactic patterns to appear.

Phyllotaxis describes the way the elements of a vegetal substance organize. The global structure is produced by an iterative process of replication of elementary material at different sites and the growth is mainly described by two parameters, the radial expansion Δr and the angle ϕ between two elements appearing consecutively. When looking at plants, different growth modes can be identified. A convenient way to represent them is by using a view from above, called the floral arrangement, in which the elements that appeared earlier are disposed on larger circles. The vegetal elements are generally located at the intersections of two sets of spirals, with i and j the numbers of spirals in each set. The whorled modes are particular cases with $i = j$. To illustrate these notions, the upper part of Fig. 1 reports a few examples of phyllotactic modes. The distichous mode in Fig. 1(a), and its corresponding floral diagram in Fig. 1(b), shows leaves organized along a cylindrical stem, $\phi = 180^\circ$. Figures 1(c) and 1(d) are the floral diagrams of modes with $i = j = 2, \phi = 90^\circ$ (decussate mode) and $i = j = 3$, $\phi = 120^\circ$ (tricussate mode), respectively. In nature, modes with angles that are not commensurate to 2π are also observed. In particular, the mode with the golden angle ϕ_g emerges, with ϕ_g linked with the golden number number $\tau = (1 + \sqrt{5})/2$ as $\phi_g = 360/(1 + \tau) \approx 137.5^\circ$. A floral diagram for $\phi \sim \phi_g$ is shown in Fig. 1(e). Remarkably, the numbers of spirals in each set are part of the Fibonacci sequence $S_F = (1,1,2,3,5,8,13,21,34,\ldots)$. The reason why Fibonacci spirals appear so frequently and in many different systems is not yet completely understood, nevertheless, several phyllotactic phase diagrams exhibit a ϕ_g divergence for large intervals of the control parameters, thus showing that golden spirals are robust growth modes [4–6].

Our experimental setup consists of a liquid crystal light valve (LCLV), with nonlocal feedback, as schematically represented in Fig. 1(f). The LCLV is made of a thin nematic liquid crystal layer placed in between a glass plate and a mirror over which a photoconductive material is deposited. The inner wall of the glass plate and the outer surface of the photoconductor are covered with a transparent conductive layer that allows applying a voltage across the cell. Liquid crystal molecules tend on average to align along the direction defined by the applied electric field and, in doing this, induce a phase retardation on the incoming beam because of their

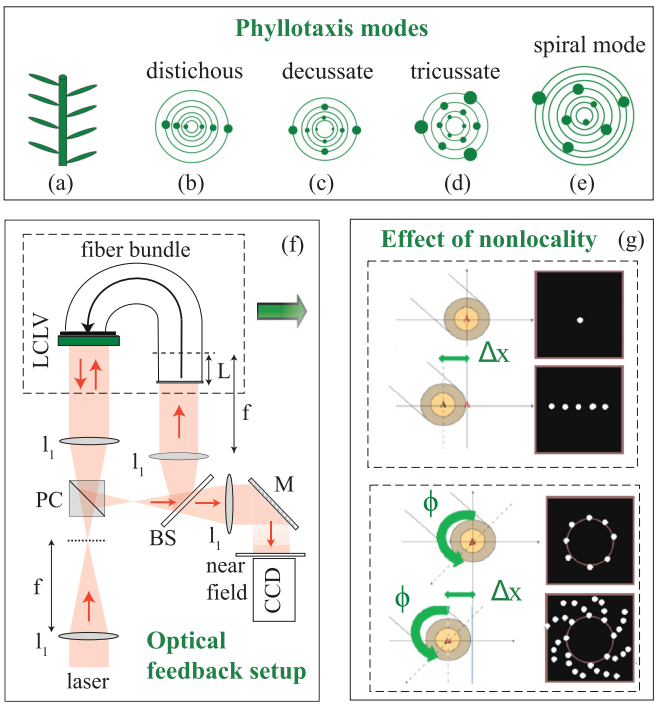

FIG. 1. (Color online) (a) Distichous phyllotactic mode for leaves along a stem and (b) its corresponding floral diagram; the divergence angle is $\phi = 180°$. Floral diagrams for (c) decussate, $\phi = 90°$, (d) tricussate, $\phi = 120°$, and (e) spiral, $\phi = \phi_g$, modes. (f) Liquid crystal light valve, LCLV, experiment; l_1 are lenses with $f = 25$ cm focal length; PC: polarizing cube; BS: beam splitter; M: mirror; L: optical free propagation length. (g) Influence of the fiber bundle displacement (left) on the localized structures observed in the near field (right).

birefringence. In the optical feedback setup, the incoming light beam is reflected back by the mirror inside the LCLV, and then it travels along the loop and goes back to the photoconductor owing to an optical fiber bundle connected to the rear side of the LCLV. The photoconductor behaves as a variable impedance with respect to the intensity of the light, hence it locally modulates the electric field applied across the liquid crystal molecules depending on the incident light intensity. Localized structures (LSs) form on the transverse optical wavefront when diffraction and polarization interference are simultaneously present in the feedback loop. In these conditions, the system becomes bistable and elementary optical elements can be locally excited [17]. Their typical transverse size scales as $(\lambda|L|)^{1/2}$, where L is the free propagation length in the feedback loop and λ the optical wavelength.

The phyllotactic patterns are observed in the near field (plane conjugated with the photoconductive side of the LCLV) and recorded with a charged coupled device (CCD) camera. They are obtained by introducing a rotation and a displacement of the feedback beam with respect to its position at the front side of the LCLV. This is achieved by, correspondingly, rotating and translating the entrance plane of the fiber bundle of an angle $\Delta\phi$ and a translation Δx, as schematically represented in Fig. 1(g). In this way, it is possible to couple different spatial regions of the LCLV and to induce spatial organizations of LSs. Previous studies reporting nonlocal effects in the LCLV experiments were presented in Refs. [18–25]. For rotations $\phi = 2\pi/m$ without any effective translational effect, the resulting pattern is made of circles with a multiple of m LSs on each ring [23]. If a small shift $\delta\phi$ exists, the circle starts to rotate in a given direction. If an effective translation Δx is introduced, the arrangements of LSs open up to describe spirals, as observed in our case. Examples of nonlocal feedback, respectively, a purely translational mode (top), a circular mode (center), and a spiral mode (bottom), are shown in Fig. 1(g).

To better illustrate that the setup realizes a geometrical distribution of LSs, we introduce a simple model consisting of a replication algorithm that places small disks, referred to as particles, on successive spatial sites. The radial position of the first particle is called R. A rotation ϕ and a radial expansion Δr are introduced between two successive sites. The position of the kth added particle is defined by (x_k, y_k), $x_k = x_c + (R + k\,\Delta r)\cos(k\phi)$, $y_k = y_c + (R + k\,\Delta r)\sin(k\phi)$, where (x_c, y_c) are the coordinates of the center. The size of the particles is noted d, their number n, and N is the size of the square system. For comparison with the geometrical model, the experimental value of ϕ is estimated by measuring with a graduate stage the rotation from a reference situation. Figure 2 shows three examples of observed phyllotactic patterns and their corresponding geometrical arrangements. In this figure and the following ones, all the experimental pictures are presented with inverted grayscale. In Fig. 2(a), $\phi \simeq 10°$–$20°$ and the LSs are organizing along a single spiral. Near the center, the distance between the adjacent LSs becomes smaller than their characteristic size ($\Lambda \sim 140\ \mu$m), hence they attach one after the other, forming lines, an effect already observed in the presence of drift [25]. When traveling along the spiral to the periphery, the distance between LSs increases and they detach one from the other, becoming independent. Figure 2(b) corresponds to $\phi \simeq 120°$. Here, the LSs organize on three spirals. Figure 2(c) is for $\phi \simeq 180°$, and the LSs are distributed on two spirals. Geometrical distributions obtained with the

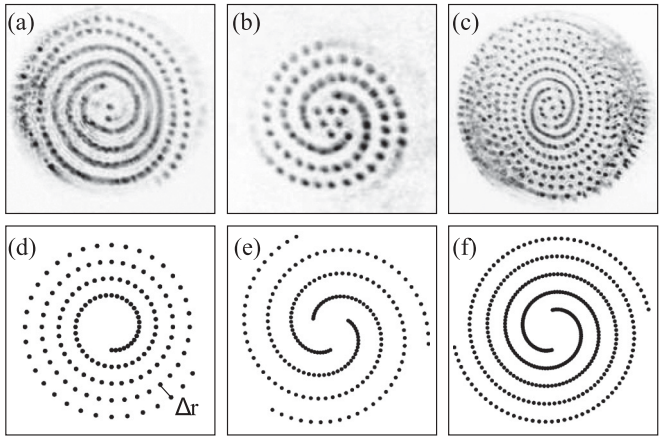

FIG. 2. Spiraling phyllotactic arrangements of optical localized structures: (a)–(c) Experimental snapshots; (d)–(f) corresponding geometrical distributions, $R = 100$, $dr = 2$, $N = 1000$. (a) $\phi \simeq 10°$–$20°$, $V_0 = 5.355$ V, $I_{in} = 590\ \mu$W/cm^2; (b) $\phi \simeq 120°$, $V_0 = 5.086$ V, $I_{in} = 475\ \mu$W/cm^2; (c) $\phi \simeq 180°$, $V_0 = 5.345$ V, $I_{in} = 1.03$ mW/cm^2; (d) $\phi = 10°$, $n = 150$; (e) $\phi = 118°$, $n = 200$; (f) $\phi = 178°$, $n = 400$.

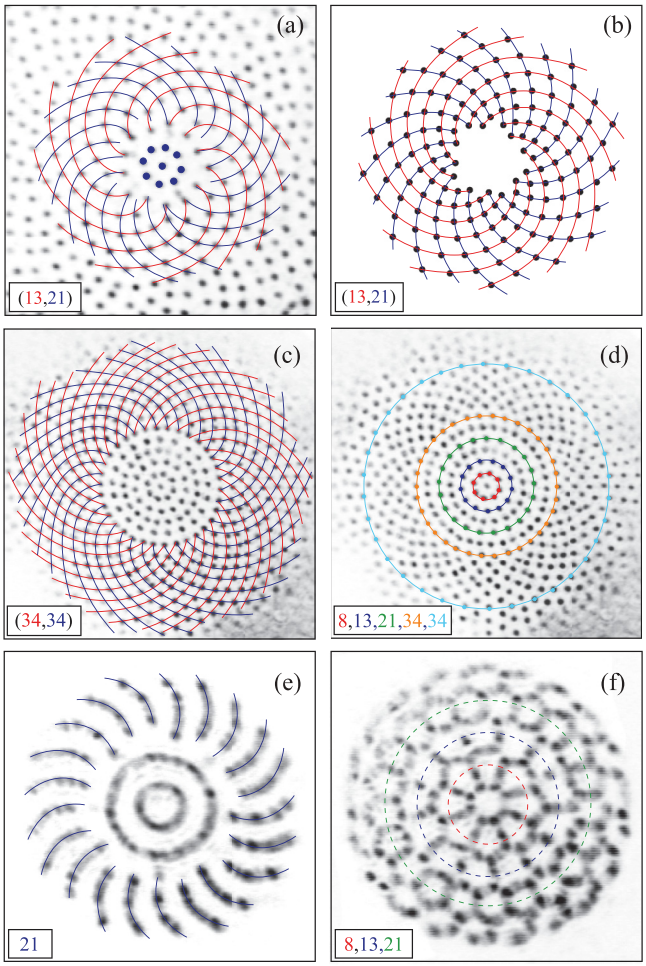

FIG. 3. (Color online) Golden spiral organizations obtained for $\phi \sim \phi_g$. (a), (c), (d) Experimental snapshots; $I_{\text{in}} = 180\ \mu\text{W/cm}^2$, localized structures (LSs) of 140 μm size. (a) $V_0 = 6.706$ V; (c), (d) $V_0 = 6.752$ V; (b) numerical profile; $d = 10, n = 150, N = 1000$, $R = 100$, $dr = 2$. In (a)–(c) the lines show the two sets of spirals at the intersection of which the LSs are positioned; in (d) the positioning of LSs is evidenced by concentric circles; on each circle the number of LSs is a term of the Fibonacci sequence. (e), (f) Organizations observed for LSs of 110 μm size; (e) sunlike arrangement with 21 spiraling rays, $V_0 = 4.947$ V; (f) flowerlike structure with the number of petals on concentric circles following the Fibonacci sequence, $V_0 = 4.957$ V.

replication algorithm and with angles close to the experimental ones are displayed in Figs. 2(d)–2(f), showing a quite good agreement with the experimental patterns.

Let us now examine the situation when ϕ is close to the golden angle. In a first set of observations the characteristic size of the LSs is $\Lambda \sim 140\ \mu$m ($L = -5$ cm in the feedback loop). An example of the pattern observed in this case is shown in Fig. 3(a). For comparison, a numerical pattern obtained numerically for $\phi = \phi_g$ is displayed in Fig. 3(b). Both in the experimental and geometrical pattern the elements are organized in two sets of spirals (i, j), with $i = 13$ in the clockwise direction and $j = 21$ in the counterclockwise direction. It is worth noting that (i, j) are two terms of the Fibonacci sequence. Another phyllotactic pattern obtained for $\phi \sim \phi_g$ and with similar experimental parameters but a

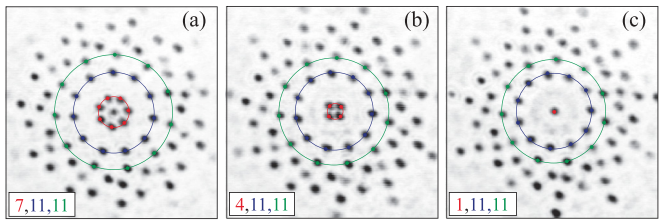

FIG. 4. (Color online) Optical organizations observed for $\phi \sim 99^\circ$; the snapshots are part of the same temporal sequence, $V_0 = 5.048$ V, $I_{\text{in}} = 490\ \mu\text{W/cm}^2$.

slightly higher V_0 is shown in Figs. 3(c) and 3(d). The same experimental profile is presented in Fig. 3(c) with evidence of the two sets of 34 spirals at the intersections of which the LSs are located and in Fig. 3(d) with evidence of the concentric circles onto which the LSs are organized. Starting from the center of the pattern, the number of LSs on each circle is a term of the Fibonacci sequence S_F, ranging from 8 to 34. For a smaller size of the LS, $\Lambda \sim 110\ \mu$m ($L = -3$ cm), we observe peculiar organizations, as the ones illustrated in Figs. 3(e) and 3(f). In Fig. 3(e) the LSs dispose themselves in a sunlike arrangement with a single spiral of 21 arms, while in Fig. 3(f), for the same light intensity but a slightly higher voltage, the LSs form a flowerlike structure with petals. It is interesting to note the way in which the petals are following the Fibonacci sequence on the pattern, with eight petals on the first circle, then 13 and 21 on the next levels.

Finally, Figs. 4 and 5 present examples of phyllotactic patterns obtained for different rotation angles, related to other divergences, and hence to other sequences ruling the geometrical arrangements of LSs. Indeed, the expression for

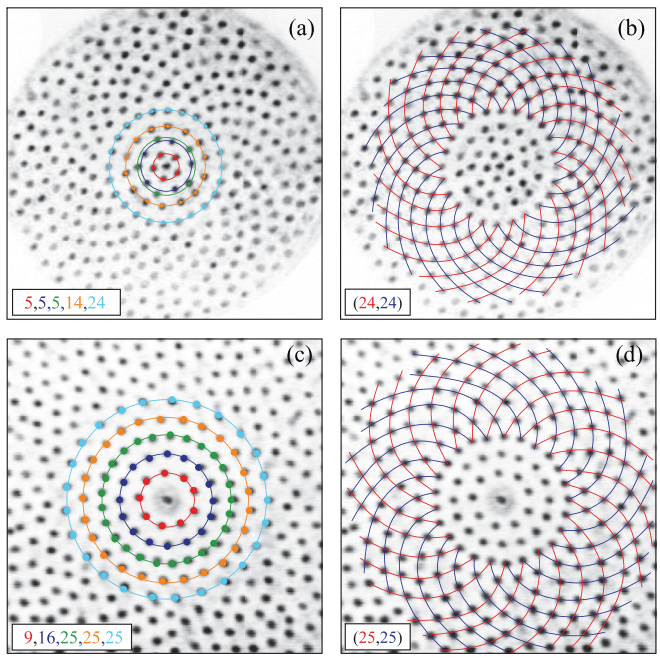

FIG. 5. (Color online) Phyllotactic patterns observed for (a), (b) $\phi \sim 78^\circ$, $V_0 = 5.087$ V, $I_{\text{in}} = 260\ \mu\text{W/cm}^2$ and (c), (d) $\phi \sim 160^\circ$, $V_0 = 6.745$ V, $I_{\text{in}} = 180\ \mu\text{W/cm}^2$. The localized structures distributions are highlighted either by concentric circles (left panels) or by two sets of spirals (right panels).

the divergence angle can be generalized to $\phi_g = 360^\circ/(p+\tau)$, which for $p \neq 1$ gives values different from the golden angle. One of the most known examples is for $p = 2$, which gives $\phi \sim 99^\circ$ and to which the Lucas sequence is associated, $S_L = (1,3,4,7,11,18,29,\ldots)$. For $p = 3$, the divergence angle is close to 78° and the associated sequence is $(1,4,5,9,14,23,\ldots)$. The cases $p = 2$ and 3 are sometimes referred to as the second and third phyllotaxis. In Figs. 4(a)–4(c), we show three representative experimental snapshots obtained for $\phi \approx 99^\circ$ and belonging to the same temporal sequence. We highlight the positions of the LSs by concentric circles. The number of LSs appearing on the first circles is 1, 4, or 7 and then 11 on the next circles, which are consecutive terms of the Lucas sequence.

The patterns obtained for a divergence angle $\phi \sim 78^\circ$ are shown in Fig. 5, with the circles and the spirals highlighted in Figs. 5(a) and 5(b), respectively. One can notice the presence of one structure in the center, five on the next three circles, and 14 on the following one, a sequence that is a part of the expected series $(1,4,5,9,14,23,\ldots)$. More at the periphery of the pattern, the LSs rearrange themselves in two sets of spirals with $i = j = 24$, with a shift of one in the number of spirals when compared to the expected term of the sequence. Finally, Figs. 5(c) and 5(d) display the patterns obtained for $\phi \sim 160^\circ$, with the circles and the spirals drawn in Figs. 5(c) and 5(d), respectively. For $\phi \sim 160^\circ$ a pattern with nine structures on the first circle, 16 on the second circle, and 25 on the following ones is expected, realizing part of a sequence with 2 as a first term and 7 as the second one, $(2,7,9,16,25,\ldots)$. Parts of the predicted occupation numbers are observed at the center of the pattern, whereas in the outer regions the LSs dispose themselves on two sets of spirals with $i = j = 25$, a number belonging to the expected sequence.

In conclusion, we have reported self-organizations of optical structures that present strong analogies with the growth modes observed in the vegetal world. The experiment, consisting of a LCLV with nonlocal feedback, allows the excitation of single optical elements thanks to the bistable features that characterize the light-matter interaction. The growth modes are selected by imposing a suitable amount of angular divergence and translation in the feedback loop. For divergences close to the golden angle, the optical elements dispose themselves on arrangements ruled by terms of the Fibonacci sequence. For other divergences, optical organizations with different symmetries are obtained.

We acknowledge financial support from the ANR international program, Project No. ANR-2010-INTB-402-02, "COLORS".

[1] See, e.g., C. Bowman and A. C. Newell, Rev. Mod. Phys. **70**, 289 (1998).
[2] P. D. Shipman and A. C. Newell, Phys. Rev. Lett. **92**, 168102 (2004).
[3] S. Douady and Y. Couder, Phys. Rev. Lett. **68**, 2098 (1992).
[4] S. Douady and S. Couder, J. Theor. Biol. **178**, 255 (1996).
[5] S. Douady and Y. Couder, J. Theor. Biol. **178**, 275 (1996).
[6] S. Douady and Y. Couder, J. Theor. Biol. **178**, 295 (1996).
[7] P. Atela, C. Golé, and S. A. Hotton, J. Nonlinear Sci. **12**, 641 (2002).
[8] J. Dumais, Curr. Opin. Plant Biol. **10**, 58 (2007).
[9] N. Rivier, R. Occelli, J. Pantaloni, and A. Lissowski, J. Phys. (Paris) **45**, 49 (1984).
[10] L. S. Levitov, Phys. Rev. Lett. **66**, 224 (1991).
[11] L. Chaorong, J. Ailing, and Z. Cao, Science **309**, 909 (2005).
[12] L. Chaorong, J. Ailing, and Z. Cao, Appl. Phys. Lett. **90**, 164102 (2007).
[13] C. Nisoli, Phys. Rev. E **80**, 026110 (2009).
[14] C. Nisoli, N. M. Gabor, P. E. Lammert, J. D. Maynard, and V. H. Crespi, Phys. Rev. E **81**, 046107 (2010).
[15] M. Mihailescu, A. D. Preda, E. Cojoc, E. Scarlat, and L. Preda, Opt. Lasers Eng. **46**, 802 (2008).
[16] M. Mihailescu, Opt. Express **18**, 12526 (2010).
[17] S. Residori, Phys. Rep. **416**, 201 (2005).
[18] S. A. Akhmanov, M. A. Vorontsov, V. Y. Ivanov, A. V. Larichev, and N. I. Zheleznykh, J. Opt. Soc. Am. B **9**, 78 (1992).
[19] P. L. Ramazza, S. Residori, E. Pampaloni, and A. V. Larichev, Phys. Rev. A **53**, 400 (1996); **54**, 982(E) (1996).
[20] E. Pampaloni, S. Residori, and F. T. Arecchi, Europhys. Lett. **24**, 647 (1994).
[21] E. Pampaloni, S. Residori, S. Soria, and F. T. Arecchi, Phys. Rev. Lett. **78**, 1042 (1997).
[22] S. Residori, N. Olivi-Tran, and E. Pampaloni, Eur. Phys. J. D **12**, 15 (2000).
[23] S. Residori, T. Nagaya, and A. Petrossian, Eur. Phys. Lett. **63**, 531 (2003).
[24] S. Residori, P. L. Ramazza, E. Pampaloni, S. Boccaletti, and F. T. Arecchi, Phys. Rev. Lett. **76**, 1063 (1996).
[25] F. Haudin, R. G. Rojas, U. Bortolozzo, M. G. Clerc, and S. Residori, Phys. Rev. Lett. **106**, 063901 (2011).